Surface Roughness and Dimensional Tolerances in A319 Alloy Samples Produced by Rapid Investment Casting Process Based on Fused Filament Fabrication

Konstantin Fedorov[1], Kazem Fayazbakhsh[1]*, Comondore Ravindran[2]
[1]Department of Aerospace Engineering, Ryerson University, Toronto, Ontario M5B2K3, Canada
[2]Mechanical and Industrial Engineering, Ryerson University, Toronto, Ontario M5B2K3, Canada
*Corresponding author: kazem@ryerson.ca; Tel: (+1) 416-979-5000 ext. 556414; fax: (+1) 416-979-5056; https://orcid.org/0000-0003-3963-8282

Abstract
Rapid investment casting can reduce cost and lead time and enables the manufacturing of more complex geometries compared to the conventional investment casting process. These advantages are offset by stair-stepping, poor burnout characteristics, and ash residue of 3D printed patterns that have a detrimental impact on surface roughness and dimensional tolerances of castings. In this work, we propose a specimen with eleven surface angles and can be 3D printed without supports to explore the effects of burnout temperature and stair-stepping on the cast surface roughness and tolerances. Patterns are 3D printed from Acrylonitrile Butadiene Styrene (ABS), Polylactic Acid (PLA), and Poly Vinyl Butyral (PVB) using fused filament fabrication. Three specimens of each material are invested in the ceramic shell, burned out at temperatures of 700, 900, and 1100 °C, and A319 alloy is cast subsequently. The original specimens and their castings are optically scanned to compare their roughness distributions and dimensional tolerances. Surface roughness average (Ra) is found to be evenly distributed for all face angles and burnout temperatures with an average value of 5 µm. Texture aspect ratio parameter (Str) shows that PVB-derived castings retain the as-3D printed surface texture better than ABS. Laser scans show that PVB patterns exert the lowest thermal expansion stress on the ceramic shell, while ABS is the worst-case, evident by extensive mold cracking.

Keywords
Rapid investment casting, roughness distribution, stair-stepping, cast dimensional tolerance.

The International Journal of Advanced Manufacturing Technology

https://doi.org/10.1007/s00170-021-08644-5

Abbreviations

ABS Acrylonitrile butadiene styrene
FFF Fused filament fabrication
IC Investment casting
PLA Polylactic acid
PVB Polyvinyl butyral
Ra Roughness average
RIC Rapid investment casting
SLA Stereolithography apparatus
SLS Selective laser sintering
Str Texture aspect ratio, area roughness parameter

1. Introduction

In the conventional Investment Casting (IC) process, CNC-machined dies are used to mold wax patterns, which are then invested in refractory materials to form the interior space of ceramic molds. After the divestment of wax and vitrification, the molds receive a charge of molten metal to impart a near-net-shape to the resulting casting. Surface roughness and geometric tolerance are critical metrics for gaging quality and defining acceptance requirements of investment-cast parts in aerospace, automotive, medical, and other industries [1-3]. They are tightly controlled parameters for applications such as pump housings, impellers, and heat exchangers where fluid flow is affected by the surface finish. Roughness is also a major factor in biomedical implants and for hand-held components where aesthetics and comfort are important. The cast surface quality and geometric tolerance in the IC process are determined by factors such as surface roughness of the wax pattern, alloy composition, investment materials, etc. The combined effect of these factors on surface quality and tolerance have been investigated in the past [4-6], resulting in improved understanding in the industry after more than half a century of experience in the IC industry.

CNC-machined dies can cost upwards of tens of thousands of dollars with lead times of several months [1,7]. The high cost and long lead time in the conventional workflow are a result of the die design process, CNC-machining of the die, setup of injection molding equipment, and the final wax production run [1]. For production batches of fewer than a hundred units or for parts with complex geometries, such as those created by generative design; the conventional IC process may not be suitable. The recently developed method of Rapid Investment Casting (RIC) is a more direct process, where the expendable pattern is produced by 3D printing in plastic material instead of injection-molded wax. RIC eliminates the die production stage in the casting workflow by producing the pattern directly, which can be invested and burned out as in the conventional process. RIC process can generate expendable patterns in a matter of days at a fraction of the cost. The outcome can be significant savings in resources during the product development stage, in low-volume production, and complex geometries that are difficult to produce by injection molding.

RIC patterns are made by rapid prototyping methods, such as Fused Filament Fabrication (FFF), Selective Laser Sintering (SLS), and Stereolithography Apparatus (SLA), of which the most economical route that can also accommodate a large-scale format is the FFF technique. The advantages of RIC are offset by limitations of 3D printing stemming from rough surface finish produced by the so-called stair-stepping effect and the behavior of 3D printing materials during burnout. Due to differences in material properties of 3D printed patterns compared with the conventional foundry wax, degradation of surface

quality and dimensional tolerances is introduced in RIC castings. The three notable causes are the stair-stepping effect inherent in any layered manufacturing process [8-12], cracking and distortion of ceramic shell by the hard polymer pattern during burnout, and reactions of molten alloy with the ash residue left after burnout [9,13].

Stair-stepping effect on surface roughness of 3D printed parts has been analyzed in detail by Reeves and Cobb [10] by comparing the actual surface roughness of a multi-faceted specimen to a theoretical roughness model developed for SLA. The specimen contained a range of facets with varying orientation angles from 0° to 180° in two-degree increments. Roughness measurement on each face was plotted relative to surface angle to obtain a roughness distribution plot for a particular set of printing parameters. The purpose of the plot was to establish a range of surface angles in which overall part roughness would be acceptable. The method devised by Reeves and Cobb [10] has since been applied for other 3D printing methods [8, 9] due to its efficiency in mapping overall specimen roughness for different combinations of process parameters. The generated roughness plots can then be used to find optimal part orientations on a printer bed to minimize roughness on critical surfaces [14].

In the case of FFF printing, as described by Di Angelo et. al. [11], the overall surface roughness due to stair-stepping is influenced by two factors: the layer thickness and the layer profile. Layer thickness is a printing setting that can be controlled directly, while layer profile is a combined function of parameters, such as nozzle diameter and temperature, extrusion rate, and the viscoelastic behavior of the extruded material [11]. The relationships between 3D printing parameters and surface roughness, and techniques for mitigating roughness have been studied in-depth for plastic parts, such as in research work by Ahn. et al. [12]. Other researchers focused primarily on the smoothing of ABS patterns produced by FFF prior to casting [15-17]. The majority of studies on surface quality in RIC have been performed for ABS patterns produced by the FFF method and appear to have used this material as an established precedent [7,17-19]. With the recent availability of numerous other printing feedstock for FFF, further research may find more suitable materials for RIC. Some of these feedstocks have been specially developed for RIC [20-23], e.g., PolyCast^{TM}, and may produce better cast surface quality and tolerances than ABS. There is limited published research on measuring changes from the as-3D printed part roughness to that of the as-cast part. However, the established methodology of generating roughness distributions in 3D printed thermoplastic specimens can be applied to cast specimens made by RIC as well.

The second issue encountered in the RIC process is cracking of the ceramic shell due to thermal expansion of FFF pattern materials. Since most FFF 3D printing feedstock such as ABS and PLA have longer polymer chains than standard paraffin foundry waxes, they tend to have wider softening curves, higher melting points and are more prone to incomplete burnout when compared to wax [13,24,25]. This may result in changes to surface roughness and dimensional tolerances of cast specimens from the as-3D printed values. Tolerance may be affected by cracking of the investment due to thermal expansion mismatch between the pattern and investment materials [9,26-28]. In RIC, 3D printed pattern expansion can cause cracking of ceramic shell due to higher melting temperatures and more importantly higher Young's modulus of thermoplastic plastic polymers, like PLA and ABS, compared to wax. The larger Young's modulus of FFF 3D printed patterns may cause breakage of fine features in the investment because of non-uniform expansion forces when the pattern is heating up. Prior to vitrification, the unfired ceramic shell is prone to some plastic deformation before the occurrence of cracking [1]. Materials with higher Young's modulus will exert more pressure on the investment walls,

causing a bulging type of distortion on flat surfaces and cracking in the corners of a pattern [9, 26,27]. Any distortion and cracking of the shell during burnout will be permanently transferred to the casting geometry as a loss of tolerance and can be non-uniform throughout the pattern. Therefore, feedstock materials with lower Young's modulus are more desirable in RIC to minimize shell distortion and cracking [9,26,27].

The last issue encountered in RIC is the ash residue left after the burnout, which can react with the melt and form a pitted surface [13,24]. RIC feedstock materials, such as ABS, have a greater tendency to be pyrolyzed than wax, leaving ash deposits in the investment, which may react with molten metal [9,13,24]. Pitting defects from any remaining ash residue tend to be randomly distributed on the cast surface or may form interior inclusions if any ash particles become dislodged from the investment by the flowing metal [1,13]. Higher burnout temperatures and longer durations may be required to eliminate most of the ash. The optimal burnout temperature and duration in RIC are therefore parameters that require further investigation for mitigation of ash defects.

The present study investigates the impact of stair-stepping, pattern material, and burnout temperature on surface roughness and dimensional tolerances of FFF 3D printed patterns and their corresponding castings. In the following sections, first, a new specimen is designed that includes eleven surface angles to explore the stair-stepping effect. Then, patterns are 3D printed from three feedstock materials, and three burnout temperatures were considered, followed by casting of the samples. Two quantitative parameters for surface roughness and two parameters for dimensional tolerances are defined. Finally, the impact of the surface angle, feedstock material, and burnout temperature on surface roughness and dimensional tolerances of plastic patterns and their corresponding castings are discussed both qualitatively and quantitatively.

2. Methodology

2.1. RIC pattern material, design, and 3D printing

Three RIC pattern materials were chosen for this study: ABS, PLA, and PVB. ABS was selected as it was the material of choice for the majority of research work on RIC patterns produced by FFF 3D printing [7,17-19]. Although studies have shown that it may not be the most suitable material due to higher residual ash content when compared to other feedstocks [24,25]. PLA is a preferred printing material due to low distortion during printing and ease of achieving a good surface finish in 3D printed patterns. Other researchers have also shown that it generates fewer ash deposits compared to ABS [24, 25]. As a result, PLA is included in the study due to its ubiquitous presence and familiarity in the 3D printing community. The last material is a special FFF feedstock made commercially available for RIC applications and trademarked as PolyCast™. It is based on Polyvinyl Butyral (PVB) and advertised to have a low ash content of 0.003% [23] while having the same advantageous 3D printing characteristics as PLA. Mechanical and thermal properties of the three materials are listed in Table 1.

Table 1. Mechanical and thermal properties of pattern materials.

Physical Property	ABS – 3D Printing Canada - Natural	PLA – NatureWorks Ingeo™ Biopolymer 4043d	PVB – ColorFab PolyCast™
Density	1.03 g/cm^3	1.24 g/cm^3	1.1 g/cm^3
$T_{Glass\ Transition}$	97 °C	55-60 °C	70 °C
$T_{Melting}$	220-240 °C	145-160 °C	130-160 °C
Young's Modulus	2030 MPa	3600 MPa	1594-1896 MPa

Yield Strength	43.6 MPa	60 MPa	34-37.4 MPa

The specimen chosen for this study is a modified version of the specimen developed by Reeves and Cobb [10] and contains eleven angled surfaces (Fig. 1a). The specimen geometry is comprised of four square-shaped elements rotated at 12.8° from one another. Each element contains three measurable surfaces, together spanning a range from 0° to 128.4° for a total of eleven surfaces (0°, 12.8°, 25.6°, 38.4°, 51.6°, 64.4°, 77.2°, 90°, 102.8°, 115.6°, 128.4°). The original roughness specimen developed by Reeves and Cobb [10] had 23 square elements in 2-degree intervals rotated about the center, having an equal number of up and down-facing surfaces. The advantage of the simplified geometry is in the efficient arrangement of many flat faces at varying angles in one part. No supports were used on down-facing surfaces as these can greatly alter the surface roughness depending on their type, density, removal process, and finishing operations. In the literature [2,3], roughness measurements were taken on down-facing surfaces left after the removal of supports. Such operations can produce highly variable results on the surface finish due to the individual judgment and skill of an operator in the removal of supports. The down-facing surfaces were limited to an angle of 128.4°, beyond which supports would have been deemed a requirement due to layer sagging. Therefore, it was decided to leave all down-facing surfaces unsupported with the minimum surface angle set to 128.4° (Fig. 1a) and not perform any finishing operations. Each facet is 11.25 x 20 mm and the overall specimen is 45 mm long. The size of the facets being judged sufficiently large for casting defects to become visually distinguishable and for subsequent roughness measurement.

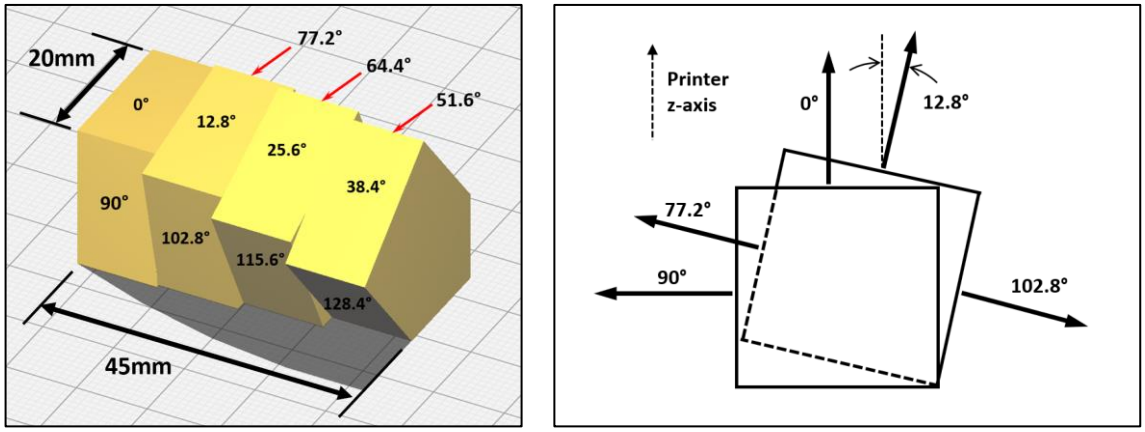

(a) (b)

Fig. 1. Specimen design for roughness measurement: (a) positions of angled faces; and (b) definition of surface orientation (its normal axis) relative to the printer z-axis (normal to the build platform).

All samples were 3D printed with Anycubic Chiron 3D printer and Cura Edition 3.2.21 was the slicer. A 0.1 mm layer height, 0.4 mm nozzle diameter, 1.5 mm wall thickness, and 15 % infill in a grid pattern were used with no support. The additional printing parameters are listed in Table 2. For casting, a set of three samples for each material were 3D printed to be used as RIC patterns, a total of nine. For measurement of surface roughness on plastic patterns, an additional set of three samples were prepared and intended for roughness measurement.

Table 2. 3D printing parameters for ABS, PLA, and PVB patterns.

Material	Design/Manufacturing Parameter	Value	Design/Manufacturing Parameter	Value

ABS	Bed temperature	100 °C	Nozzle temperature	215 °C
	Printing speed	40 mm/sec	Cooling	No fan cooling
PLA	Bed temperature	60 °C	Nozzle temperature	205 °C
	Printing speed	50 mm/sec	Cooling	Yes
PVB	Bed temperature	60 °C	Nozzle temperature	205 °C
	Printing speed	50 mm/sec	Cooling	Yes

To eliminate the effects of metallostatic pressure variation, the casting samples were oriented in a horizontal position relative to the riser and placed 150 mm below the pouring cup (Fig. 2). A set of three risers for each material were 3D printed using a 0.2 mm layer height and 0.8 mm wall thickness while all the other manufacturing parameters were the same as the ones specified previously for the RIC patterns. Each pattern sample was attached to an individual riser using a pattern assembly wax as shown in Fig. 2.

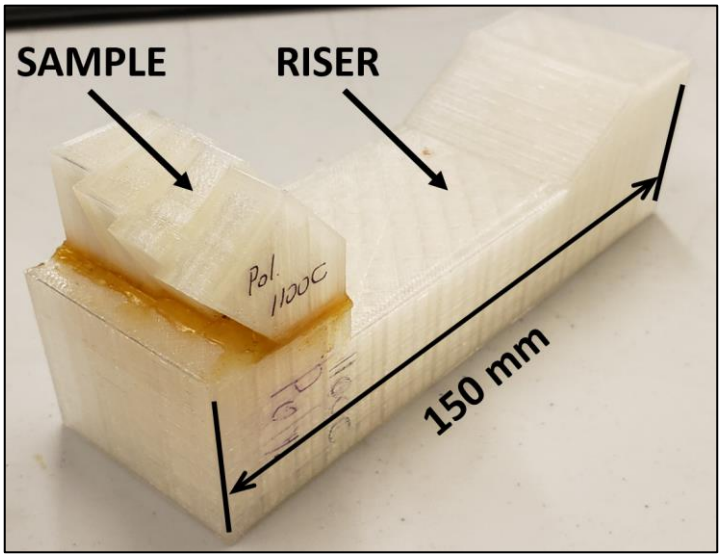

Fig. 2. PVB pattern sample attached to a riser intended for 1100 °C burnout.

2.2. Investment, burnout, and casting

The ceramic shell slurry was a premixed product based on colloidal silica (SuspendaSlurry® by Ransom & Randolph), which is designed to maintain fine refractories in suspension without the need for constant agitation. The slurry had a viscosity reading of 20 seconds measured by a no. 5 Zahn cup. The completed ceramic shell was composed of seven coatings using Suspenda-Slurry as a binder. The prime coat was prepared by dipping the pattern in the slurry, brushing the surface to remove air bubbles, followed by additional dipping and a 50/100-mesh fused silica stucco. The five backup coats were made with 30/50-mesh stucco, and the last sealing coat contained no stucco. The patterns were each given 24 hrs to dry between coatings in a 15 °C environment. The prime coat was allowed to dry naturally, while the remaining coatings were dried using forced air directed by a fan. A total of nine 3D printed patterns were made: One sample for each burnout temperature (700, 900, and 110 °C) and each material (ABS, PLA, PVB).

Prior to burnout, the kiln was preheated to the required temperature and each pattern was directly inserted into the kiln interior for a one-hour duration burnout. The kiln was of electric resistance type and equipped with a 20 x 50 mm opening that was left open for the duration of burnout with the

temperature setting kept constant. After burnout, the shells were left to cool to room temperature for inspection of shell cracking and ash residue. The process was kept identical for 700, 900, and 1100 °C burnouts. The shells were not subsequently washed out with water or compressed air with the intention of preserving any potential ash leftover on the surface. In real-world applications, it may not be possible to remove all residue from some ceramic shells due to the inability of water or compressed air to reach into deeply recessed features in the shell. Therefore, it was of interest to compare the effects of ash residue, which is left after pattern burnout at different temperatures, on the cast surface.

The Aluminum alloy chosen for the casting trials was A319 due to its wide use in the industry and castability. The individual melts were heated to 730 °C in an electric resistance furnace, degassed with Eldiron-160 degassing agent, and skimmed prior to pouring. The degasser is based on Hexachloroethane, which was added at 0.25 wt% of the alloy with a perforated plunger. Prior to pouring, the shells were pre-heated in a furnace at 800 °C for 15 minutes. The cast shells were then placed into graphite pots and allowed to cool naturally at room temperature.

2.3. Measurement of surface roughness and dimensional tolerances

Surface roughness and dimensional tolerances were measured on 3D printed patterns and cast samples. For 3D printed patterns, to provide light reflectiveness to the transparent surfaces, the samples were marked with silver ink. This modified the surfaces and made them unsuitable for investment casting. These samples were not used as RIC patterns and additional samples were 3D printed for scanning. The samples were scanned with a confocal profilometer Sensofar S Neox (Sensofar Metrology, Barcelona, Spain) at 1.38 µm resolution, to generate a roughness distribution map for each sample.

The roughness parameters selected were Ra and Str with a standard cut-off wavelength of 0.8 mm. Ra roughness values were calculated by averaging ten measurements on each facet with the individual roughness profiles aligned perpendicular to the 3D printing layer lines. The maximum stair-stepping distance in the present study was calculated to be 0.451 mm prior to printing (0.1 mm/sin12.8°) for the 12.8° facet, which is less than the 0.8 mm cut-off used for Ra measurement (Fig. 3). In the literature, large variances in roughness values were recorded for surfaces close to the horizontal, 0° and 180° [2, 3]. This variation can be explained by the conventional cut-off wavelength of 0.8 mm used by the researchers and the wide stair-stepping intervals for surface angles close to the horizontal [2,3]. By the definition of roughness average Ra, surface features greater than the characteristic cut-off wavelength will be considered waviness [29]. For low face angles on FFF 3D printed surfaces where the stair-stepping spacing is greater than the characteristic wavelength, Ra will not fully capture the roughness of a layered surface generated by the 3D printing process. Since the 3D printing layer lines impart a directional quality to surface roughness, Str roughness parameter was selected and measured from the scanned surfaces. The Str parameter (Texture Aspect Ratio) measures the correlation between roughness and directionality, ranging from zero to one. Surface roughness with a presence of directional quality (“lay”) will have Str values closer to zero. Surfaces with an isotropic roughness that is independent of direction will have Str values closer to one. For dimensional tolerances, each of the samples was scanned by a handheld laser scanner HandyScan 3D (Creaform Inc., Lévis, Canada) with an accuracy of 0.025 mm and 0.1 mm mesh. Prior to scanning, the samples were coated with powdered sugar to improve the reflectivity of transparent surfaces. The sugar coating was subsequently removed by rinsing in water prior to investing.

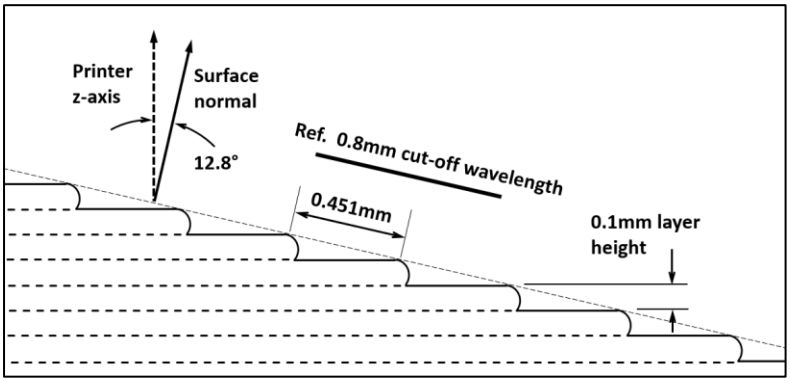

Fig. 3. Stair-stepping intervals of 0.451 mm for a 12.8° inclined surface produced by stacked layers. The characteristic cut-off wavelength of 0.8 mm is shown for comparison.

After investment, the cast samples were cut off from the risers, labeled, and scanned for surface roughness and dimensional tolerances. Roughness measurements were made using the same processes performed for 3D printed pattern samples but with the use of focus variation technique instead of confocal microscopy and without the use of coatings. The focus variation method proved better at capturing the fine surface texture of Al castings. Dimensional tolerances were also obtained using the same process as for the 3D printed pattern samples with HandyScan 3D scanner but without surface coatings. Scans of 3D printed pattern and cast samples were aligned together in VXelements software and their dimensional differences were measured.

3. Results and discussion

3.1. Visual inspection of ceramic shells and castings

After completion of burnouts, it was observed that ceramic shells derived from ABS patterns had significant cracking in the corners (Fig. 4). Castings produced by PLA patterns also displayed cracking but to a lesser degree. PVB-derived ceramic shells had no cracks on the surface and produced a high-pitched sound when tapped with a rod. ABS and PLA ceramic shells made a much duller sound, indicative of the presence of cracks. In addition to cracking, ABS and PLA-derived shells had powdery debris and flakes falling out when the shell was inverted. The debris appeared to be mostly ceramic shell powder. This resulted in erosion of the inner surfaces of ABS and PLA-derived shells, with interior air bubbles exposed on the surface. Ceramic shells made from PVB patterns showed the least powder residue and surface erosion.

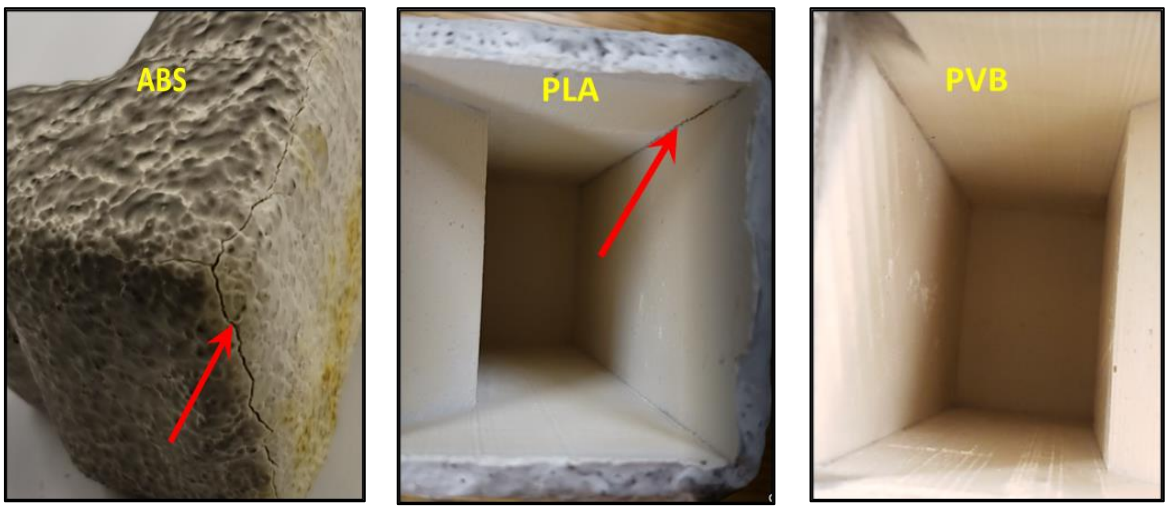

Fig. 4. Ceramic shell surfaces from different pattern materials, 900 °C burnout. Cracking on ABS and PLA-derived shells is highlighted. No visible cracking on PVB-derived shell.

The cast surfaces of PLA and PVB samples appeared very similar, with the majority of print lines preserved on all facets and some pitting distributed randomly (Fig. 5). No ash-related defects were observed on any of the surfaces. These would normally appear as gas bubbles and cavities on the surface. All of pitting on cast surfaces had rounded edges suggesting that these were formed due to surface tension of the alloy forming a meniscus around loose shell particles protruding from the mold surface. Because of the wide opening in the shell, there was no stratified airflow inside the mold, allowing any pyrolyzed carbon residues to burn out fully.

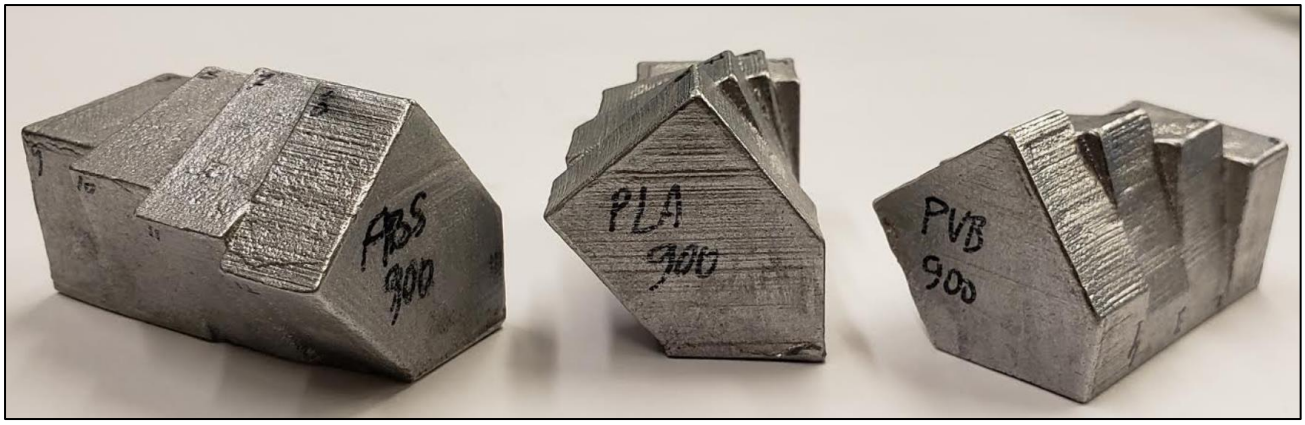

Fig. 5. Cast samples showing facets with varying surface angles, 900 °C burnout.

ABS-derived castings had more surface pitting and overall retained less of the original stair-stepping features from the original 3D printed patterns, especially on 38.4°, 51.6°, and 90° angled surfaces (Fig. 6, 7). No flashing was observed on any of the castings even though visible cracks were present on ABS and PLA-derived ceramic shells. To quantify differences in surface quality, surface roughness, and dimensional tolerances are discussed in the following sections.

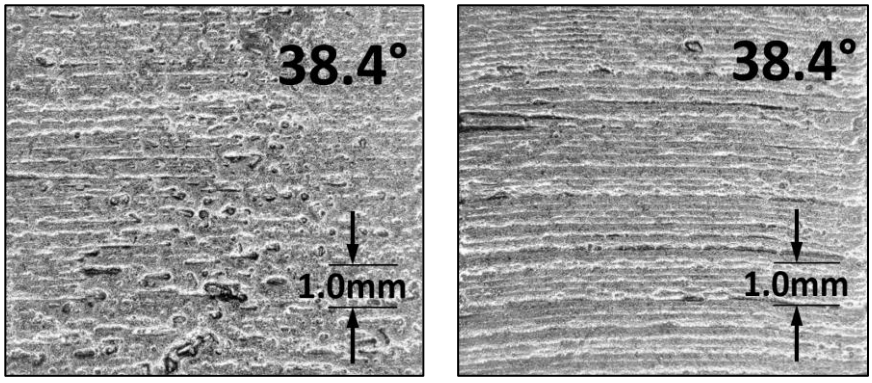

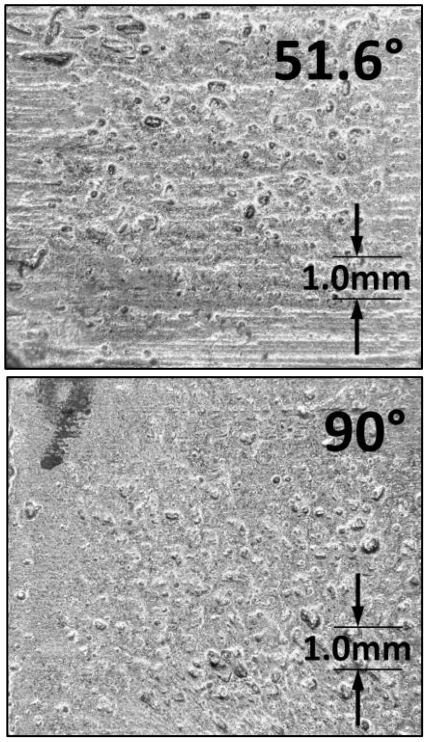

Fig. 6. ABS-derived casting surfaces for selected face angles, 700 °C burnout, showing characteristic pitting.

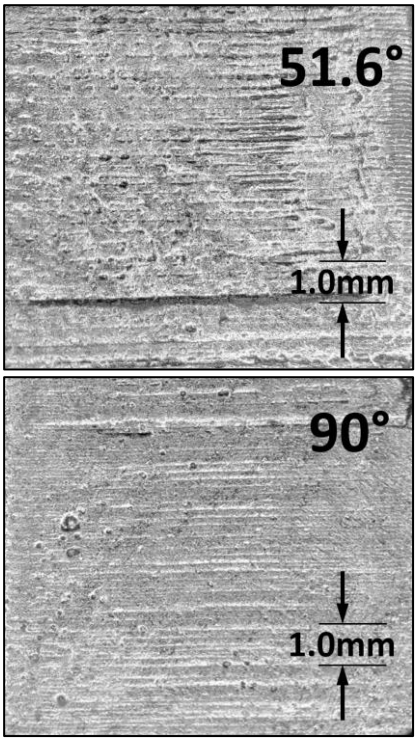

Fig. 7. PVB-derived casting surfaces for selected face angles, 700 °C burnout.

3.2 Surface roughness measurements

Fig. 8 shows Ra roughness distribution for the 3D printed pattern and cast samples for ABS, PLA, and PVB, respectively, as a function of surface angle for different burnout temperatures. It should be noted that due to excessive cracking of ABS shell at 1100 °C burnout there was no attempted casting. Ra roughness for all 3D printed patterns (dashed blue line in Fig. 8) rapidly increases from 0° to reach a peak at 12.8° (ABS and PLA) or 25.6° (PVB). Then, it reduced gradually and reached a minimum value at 90°, where it increased again with an increase in the surface angle. The maximum Ra roughness for ABS, PLA, and PVB are 15, 20, and 25 µm, respectively. The roughness distributions as a function of surface angle followed the trends observed in prior research [10-12]. Contrary to the 3D printed patterns, Ra roughness for ABS, PLA, and PVB-derived castings remains evenly flat at approximately 5µm for all surface angles. This is the case for all burnout temperatures, which appear to have little impact on the roughness distribution of cast specimens.

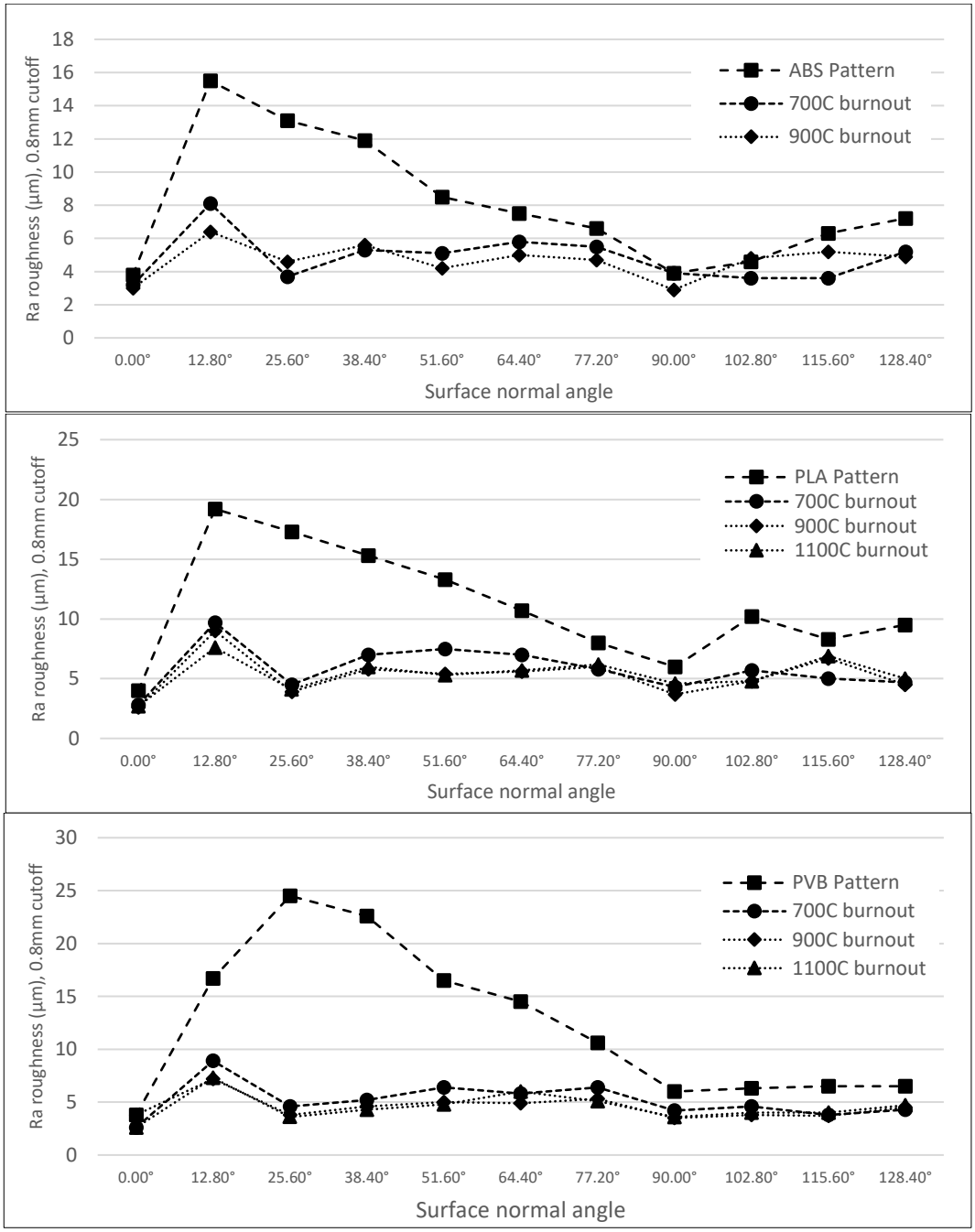

Fig. 8. Ra roughness vs. surface angle for 3D printed patterns and resulting castings: (a) ABS; (b) PLA; (c) PVB.

The flattening of the roughness distribution seen on cast surfaces can be attributed to the inability of the metal to completely fill the deep 3D printing layer line left from the original pattern in the ceramic shell. Aluminum alloys are known to display a non-wetting behavior on silica and alumina ceramic substrates due to inter-surface repulsion and high wetting angles. The high wetting angle implies that molten aluminum will not have a good filling capacity and requires a higher metallostatic head to fill the finer details of the casting such as 3D printing layer lines or small crevices left in the shell surface by erosion. The consequent smoothing effect produced by the surface tension of molten A319 alloy is therefore likely more dominant than any roughening of the shell that was observed visually. The smoothing effect can be observed on the scanned surfaces (Fig. 9) of a 25.6° facet taken from a PLA 3D printed pattern and the corresponding casting. Cast stair-stepping features are much shallower than

on the printed pattern. The same effect was observed for all other facets, showing a limit imposed on how deep the molten A319 alloy has flowed into the grooves. The result was a constant roughness for all face angles and a reduced cast roughness distribution relative to that for the 3D printed patterns.

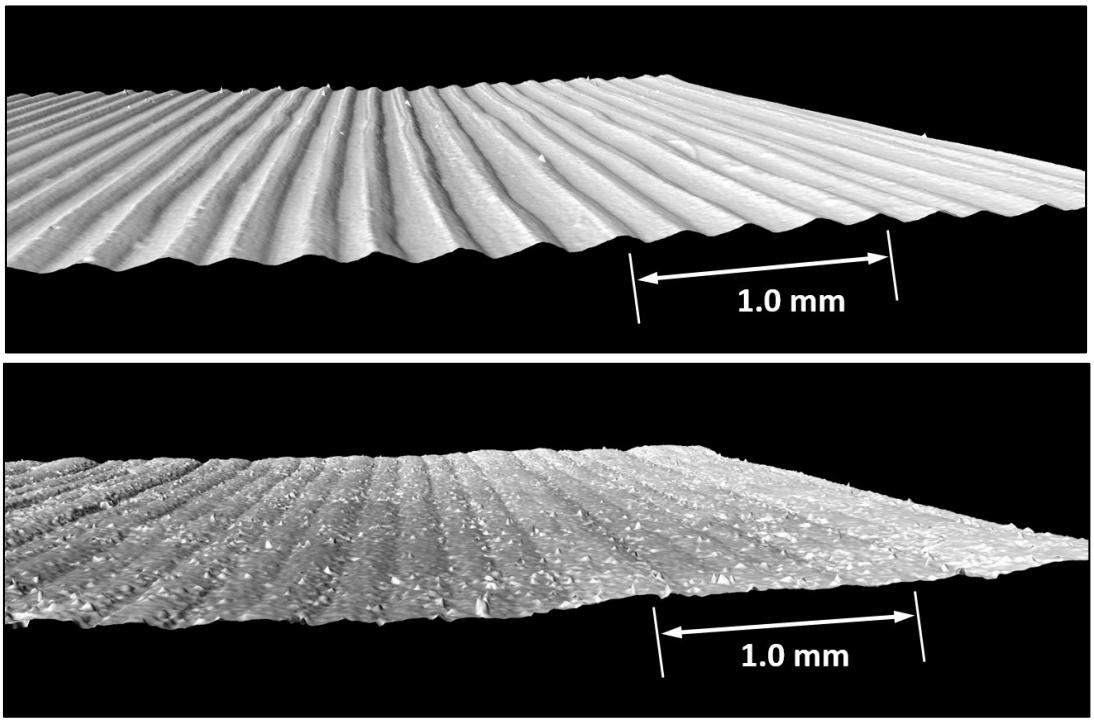

(a)

(b)

Fig. 9. Scanned images of 25.6° facet: (a) 3D printed PLA pattern; and (b) cast sample from 700 °C burnout.

Plots of roughness profiles for a 3D printed PLA pattern and the corresponding casting for a 700 °C burnout are shown in Fig. 10. The average roughness amplitude of the 3D printed surface is approximately 60 µm and it is 15 µm for the cast surface. The decrease in roughness can be attributed to insufficient metallostatic pressure to push the metal into the mold surface. Additionally, it may be explained by the breakage of the positive groove lines from the ceramic shell during burnout. There may be several reasons for the degradation of shell surfaces. Absorption of molten pattern material into the shell porosity can happen as it also takes place for the standard foundry wax during the first few seconds of burnout [1]. The subsequent evaporation of the absorbed material may exert pressure on the inner surface of the ceramic shell and cause breakage. The breakage may appear as pitting or flaking of the shell. Mechanical deformation of the pattern may cause the finer shell features such as the positive impressions of the 3D printing layer lines to break off the surface, possibly contributing to the smoothing of a roughness profile (Fig. 10).

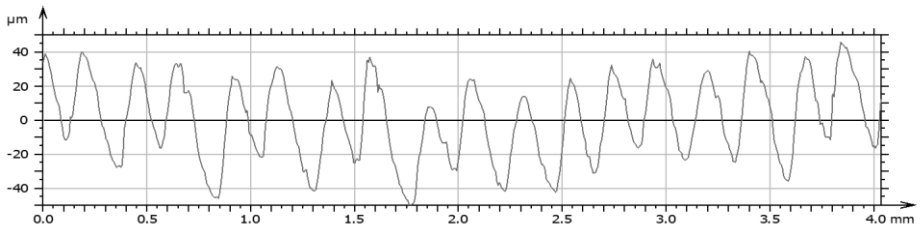

(a)

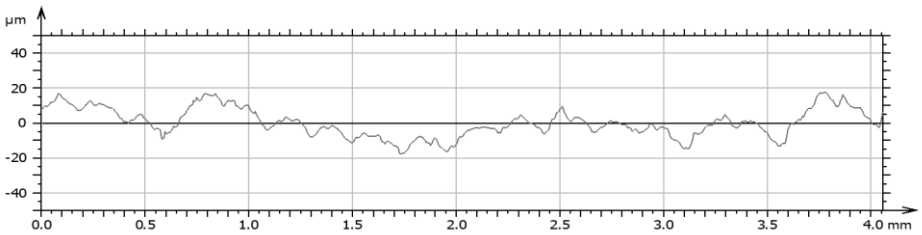

(b)

Fig. 10. Examples of a scanned roughness profile on the 25.6° facet: (a) 3D printed PLA pattern; and (b) corresponding PLA-derived casting at 700 °C burnout.

Part of the ABS-derived shell surface at 38.4° angle appears to be broken off on a 900 °C burnout sample (Fig. 11). The broken surface has a visible step-change in texture and no visible print lines, indicating that a thin layer of the ceramic shell has peeled off from the surface during burnout. The powdery white residue observed in the molds after burnout may be attributed to this loss of ceramic shell on the inner surface. Ra roughness on this facet did not allow capturing the change in surface texture or breakage.

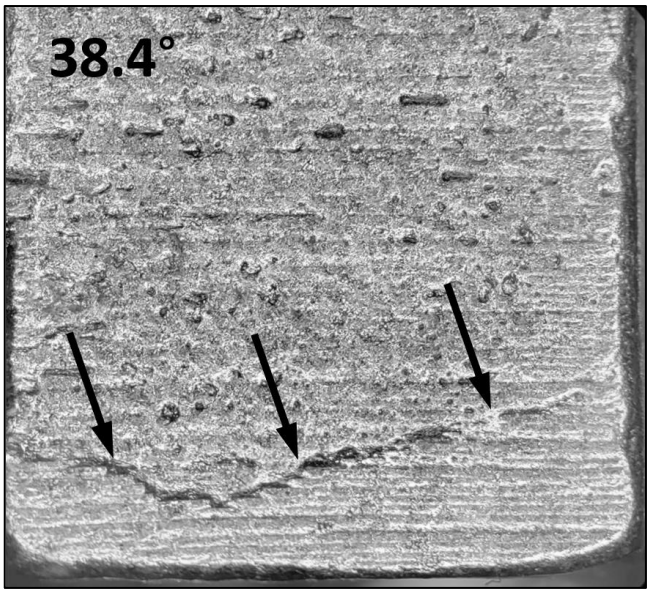

Fig. 11. Shell fracture appears as a step-change in the texture of an ABS-derived casting, 900 °C burnout sample.

In addition, a visible difference in surface texture can be visually observed between ABS and PVB-derived casting (Fig. 6, 7) that cannot be captured using Ra roughness. As a result, a different roughness parameter, Str, was used to better quantify this difference. The main difference in texture is the disappearance of print lines on the ABS-derived casting for facets with 38.4°,51.6°, and 90° angles and better preservation of these lines on a PVB-derived casting (Fig. 6, 7). A plot of Str values taken from scans of cast 700 °C samples shows smaller Str values for PVB-derived castings compared to ABS for most surface angles (Fig. 12). The Str values of original plastic patterns are all close to 0.2. As mentioned in Section 2.3, Str values closer to zero indicate surface roughness with a presence of directional quality. Therefore, it can be concluded that PVB-derived castings, in general, tend to preserve the original 3D printed pattern roughness better than ABS. The Str parameter is qualitative in nature and is thus better suited for detecting changes to directionality of cast surface texture from the original as-printed texture.

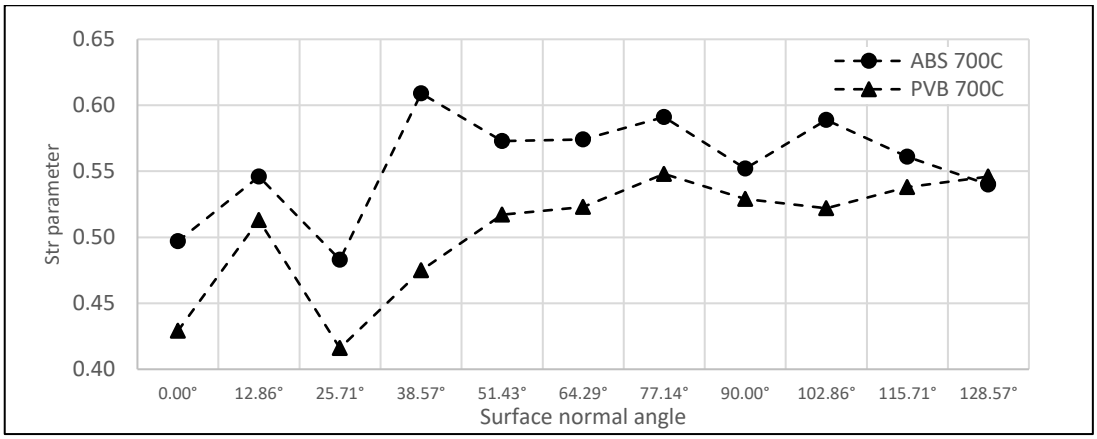

Fig. 12. Str roughness parameter vs. surface angle for ABS and PVB-derived castings, 900 °C burnout.

3.4. Theoretical description of surface tension and filling

As a result of the high surface tension of molten Al alloys and a non-wetting contact with silica, a composite interface surface (Fig. 13) of solid-liquid and solid-vapor will form as described by Eustathopoulos et. al. [30]. The contact angle between molten Al and a fused silica substrate was measured in previous literature [31] to be approximately 150° - 140° by the sessile drop method, which is strongly non-wetting (wetting angle above 90° is considered non-wetting). This was measured for a temperature range of 700° C - 800° C and for total time spent in a liquid state of less than 5 min, which is applicable to the current study. The relatively high surface tension of liquid Al was recorded to be in the range of 1-2 Nm^{-1} in both vacuum and atmosphere by Campbell [32] and Molina et. al. [33].

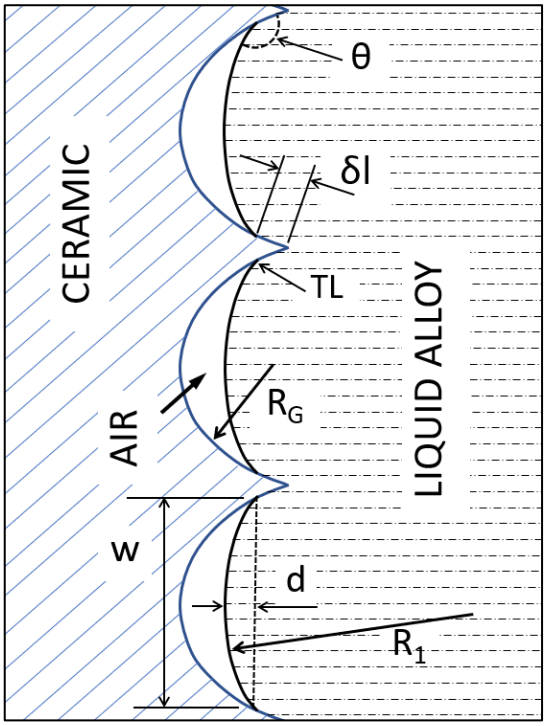

Fig. 13. Cross-section showing infiltration of the melt into the print-line grooves of the ceramic shell.

The partial filling of ceramic shell print grooves by liquid metal due to surface tension can be described with models of liquid metal surface tension and contact angles at the triple line (TL in Fig. 13). The

Laplace equation relates surface tension and radius of curvature of the liquid-vapor interface by the following relationship:

$$P_L - P_V = \sigma_{LV}\left(\frac{1}{R_1} + \frac{1}{R_2}\right) \tag{1.1}$$

, where P_L and P_V are pressures on the liquid and vapor sides of the interface, σ_{LV} is liquid-vapor surface tension, R_1 and R_2 are the principal radii of curvature. The two radii can represent any complex curvature of a compound surface that can form on a liquid drop or liquid in contact with a solid surface. In the present context, only one curvature is present R_1 (Fig. 13), with the second R_2 approaching infinity as the print line groove is a straight line. The difference in pressures P_L-P_V is equal to the metallostatic pressure ρgh, which brings equation 1.1 to:

$$\rho gh = \frac{\sigma_{LV}}{R_1} \qquad \text{or} \qquad R_1 = \frac{\sigma_{LV}}{\rho gh} \tag{1.2}$$

, where ρ is the density of the alloy (kg/m^3), g is the gravitational constant (m/s^2) and h is the metallostatic head (m). The depth of melt penetration d as a function of the width w and radius of curvature of liquid R_1 (Fig. 13), can be approximated by a formula for the sagitta of a circular arc.

$$d = R_1 - \sqrt{{R_1}^2 - \frac{w^2}{4}} \tag{1.3}$$

, where d is the sagitta, w is the chord width, and R_1 is the radius of the arc. Substituting Eq. 1.2 for R_1 we obtain:

$$d = \frac{\sigma_{LV}}{\rho gh} - \sqrt{\left(\frac{\sigma_{LV}}{\rho gh}\right)^2 - \frac{w^2}{4}} \tag{1.4}$$

Approximating w to equal the print line width of 100 µm for 90° surface and taking values of 1 Nm^{-1} for σ_{LV} [32], ρ = 2700 kgm^{-3}, g = 9.81 ms^{-2}, h = 0.15 m, and w = 0.0001 m (print line width), the depth of penetration will be approximately 5 µm. This small value is suggesting that the liquid melt surface infiltrating a narrow print line channel of 100 µm is nearly flat. This is evidenced by a profilometry scan on Fig. 9(b) and 10(b) showing the flat surfaces of the solidified A319 alloy. Likewise, the average cast Ra roughness for all specimens is close to this value. Aside from penetration depth d, there is an additional distance δl that the melt will travel along the groove wall to form a partially wetted surface. Higher metallostatic pressures will have a tendency of pushing the melt into the grove via increasing distance δl and decreasing radius R_1.

The above description is applicable to most Aluminum alloys and fused-silica ceramic molds in the casting temperature range of 650° C - 800° C and a solidification time less than approx. 5 min. Different results will be seen for melt-ceramic combinations that display a wetting contact behavior or higher melt temperatures. As demonstrated by Marumo [31], the wetting angle of Al begins to drop sharply above about 750° C, dropping to 90° at 900° C. Time spent in a liquid state in contact with the ceramic will also have a strong effect on wettability and the ensuing increase of roughness. In the same paper, it was shown that contact angle decreased from 140° to 70° at 800° C after 40 minutes in a liquid state. This dramatic decrease is due to reactions between Al alloy and SiO_2 that comprises the mold. The

wetted surface is modified by deposits of reaction bi-products that form a lower wetting angle with the melt. The primary surface reactions that will take place is of the redox type [31] such as:

$$SiO_2 + 2Al \rightarrow 2AlO + Si \quad (1.5)$$
$$SiO_2 + 2AlO \rightarrow Al_2O_3 + SiO \quad (1.6)$$
$$¾SiO_2 + Al \rightarrow ½Al_2O_3 + ¾Si \quad (1.7)$$

Due to the stronger affinity of Al to the bonded oxygen atoms in fused silica, SiO_2 is reduced by Al in a set of complex reactions such as Eqs. 1.5-1.7. Leaving behind layers of complex aluminosilicate bi-products that have higher wettability than the original ceramic shell. This will manifest as a gradual spreading of the molten Al in the sessile drop method [34] and increased filling of any small features in the mold. The consequence of this for the IC process is that thicker sections with longer cooling periods and higher superheats will produce a rougher surface finish than thinner castings poured at lower temperatures.

The effect of longer cooling time and higher melt temperature may be partially counteracted by the increased surface tension of Al due to oxide skin formation. Campbell [32] showed that surface tension of molten Al alloys can nearly double due to the formation of oxide films. The increased surface tension and thicker oxide film of the melt can lessen the contact area and reactivity with the shell surface. In any case, complete filling of the print line groove in the ceramic shell should not occur until the radius of curvature R_1 drops to that of the groove radius R_G (Fig. 13) due to increasing metallostatic pressure and decreasing surface tension.

3.5. Dimensional tolerances

Dimensional differences between the 3D printed patterns (baseline) and their corresponding castings were obtained. Fig. 14 shows the differences for ABS pattern and ABS-derived casting with 900 °C burnout.

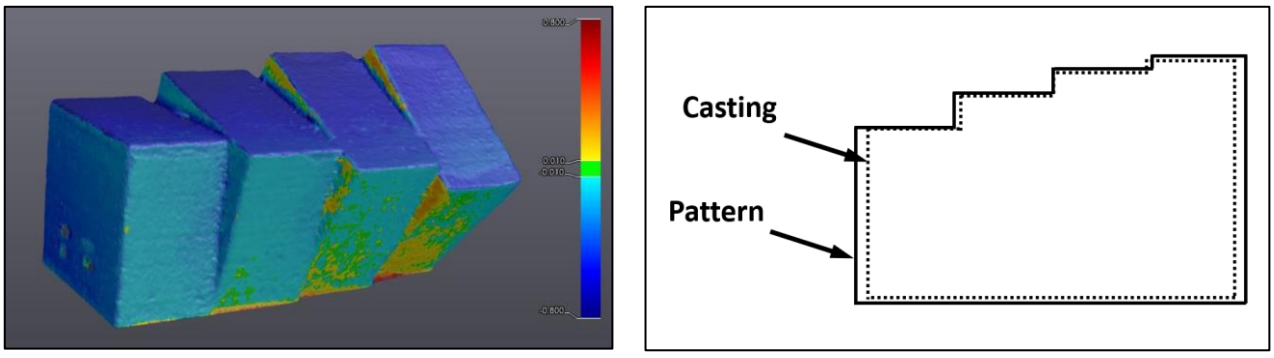

(a) (b)

Fig. 14. Dimensional differences between the 3D printed ABS pattern and its corresponding casting, 900 °C burnout: (a) 3D laser scan; (b) schematic showing shrinkage.

To compare the impact of pattern materials and burnout temperatures on dimensional tolerances, two parameters, longitudinal and transverse deviations, are defined: longitudinal deviation is a dimensional difference between the scanned 3D printed sample and its corresponding casting along the sample length, while the transverse deviation is measured across the 90° square element. Fig. 15 shows these

parameters for three pattern materials and three burnout temperatures (recall that there was no casting for ABS shell with 1100 °C burnout). The plots show that the longitudinal deviation for PVB castings averages about 0.69 mm, which amounts to 1.54 % dimensional change (0.69 mm/45 mm), and transverse deviation is 0.37 mm, or 1.86 % dimensional change (0.18 mm/20 mm). The corresponding values for 3D printed PLA patterns and their corresponding castings are close but slightly lower than those for PVB. For ABS, the dimensional variations were 0.51 % and 0.96% for longitudinal and transverse deviations, respectively.

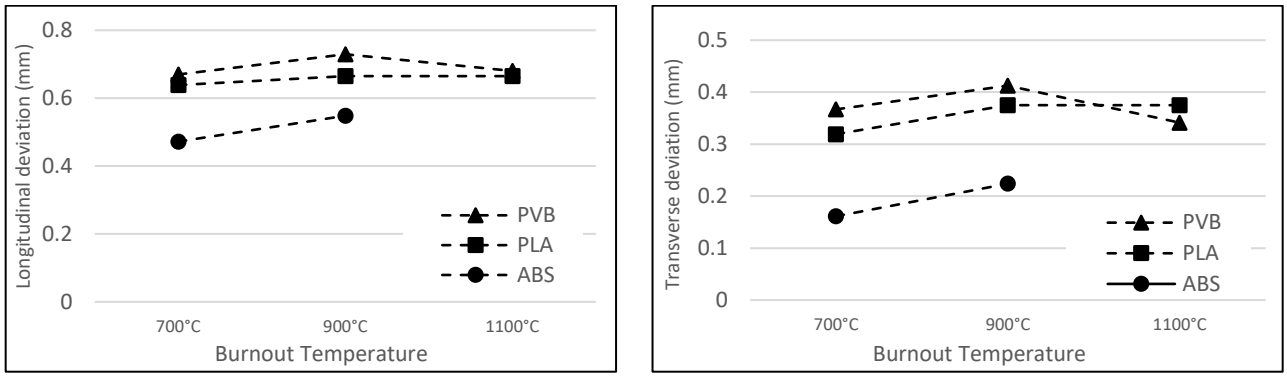

Fig. 15: Dimensional deviations of castings from their original printed patterns: (a) Longitudinal direction; and (b) Transverse direction.

In open molds, a dimensional change of approximately 2 % is expected for A319 castings due to metal cooling shrinkage. Smaller deviation values for RIC patterns indicate that pattern expansion during burnout possibly leads to ceramic shell expansion. This expansion of inner shell dimensions partially counteracts the shrinking solidification. The severe cracking observed on ABS-derived shells has led to larger shell interior dimensions, which offset cooling shrinkage to produce an average shrinkage of about 0.74 % ((0.51 % + 0.96 %) / 2). The larger deviations for PVB-derived castings of around 1.7 % indicate that shell expansion was smaller and had less effect on counteracting metal cooling shrinkage. This is also in agreement with the severe cracking observed on ABS-derived shells, lesser cracking on PLA-derived shells, and no visible cracking for PVB-derived shells.

3.6. Environmental impact of 3D printed patterns

3D printed patterns cannot be devested by the environmentally friendly autoclaving method most used with wax patterns, due to the high melting temperature of polymers. Wax has the distinct advantage that it may be collected and reused for subsequent patterns with some deterioration in properties [1]. ABS is perhaps the most damaging to both health and the environment during the manufacturing and burnout stages. It was reported to produce ultrafine particles and carcinogens such as butadiene during burnout [35]. It is not carbon neutral and is derived from petroleum [36]. PLA is the least damaging material during 3D printing and in terms of environmental impact as it is entirely derived from plant material [37]. PVB is synthesized from plant-based PVA and petroleum-derived butanal [38, 39], so it will have more impact than PLA but less than ABS. None of the above-mentioned polymers produce chlorinated by-products that will require special treatment of fumes. Combustion products of the three materials are comprised only of carbon, oxygen, and hydrogen.

4. Conclusions

Surface roughness and dimensional tolerances of FFF 3D printed thermoplastic patterns and their corresponding castings are compared qualitatively and quantitatively for different surface angles (from 0° to 128.4°), feedstock materials (ABS, PLA, and PVB), and burnout temperatures (700, 900, and 1100 °C). ABS and PLA patterns displayed severe cracking of the shell at all burnout temperatures, while PVB patterns showed the least surface erosion and powder residue. Surface texture of PVB and PLA-derived castings varies significantly from that of ABS as seen in the better-preserved stair-stepping patterns. Roughness distributions of castings as measured by the Ra parameter are flattered with an average value of 5 µm in comparison to original plastic patterns. The flattening is due to the inability of molten alloy to completely fill the stair-stepping 3D printing layer lines transferred from the plastic pattern onto the ceramic shell. For indicating loss of stair-stepping texture resulting from erosion of ceramic shell, Str roughness is a more effective roughness parameter than Ra. As demonstrated by the Str values close to those of plastic patterns for PLA and PVB, they are preferable to ABS for reducing inclusions and surface defects. Dimensional differences between the 3D printed patterns and their corresponding castings show 0.78 % and 0.9 % longitudinal and transverse changes, respectively, for PVB. These values are greater than those for ABS and PLA that show its shell expansion was smaller and had a smaller counteracting impact on metal cooling shrinkage. The present work demonstrates that the roughness distribution methodology developed for plastic components can be used for measuring cast surface roughness in the RIC process. Surface roughness analyses and dimensional tolerances in the final castings show that PVB behaves significantly better than the commonly used ABS feedstock.

To better analyze the surface degradation of inner ceramic shell surfaces, a micrographic inspection of the samples may be used. Optical microscopy of the samples may enable further analysis of the surface degradation of the inner surface of the ceramic shell. Smaller ceramic shell samples can be prepared in different pattern materials and burnout temperatures like the present study but without actual casting. Microscopy of the sectioned shells can help in assessing ceramic shell delamination, ash residues, and possible erosion on the shell surface. Additionally, any pyrolyzed polymer trapped in the inner shell layers may serve to gain a better understanding of the degree of absorption of the pattern polymer into the ceramic shell body. Friability tests can be performed on ceramic shell samples prepared by various polymers to measure resistance to abrasion of the inner shell surfaces. Ceramic shell surfaces damaged by interactions with RIC pattern materials during burnout will be abraded away more easily by the friability test.

Acknowledgments

The authors thank Dr. M. Papini for the use of the high-resolution optical surface scanners and software enabling accurate roughness analyses.

Declarations

Funding

This work was supported by the Natural Sciences and Engineering Research Council of Canada (NSERC), RGPIN-2018-04144.

Conflicts of interest/Competing interests
The authors have no conflicts of interest to declare that are relevant to the content of this article.

Availability of data and material
The authors will provide relevant documentation and/or data upon request.

Code availability
Not applicable

CRediT author statement
Konstantin Fedorov: Conceptualization, Methodology, Validation, Formal analysis, Investigation, Writing - Original Draft, Writing - Review & Editing. **Kazem Fayazbakhsh:** Resources, Writing - Original Draft, Writing - Review & Editing, Supervision, Project Administration, Funding acquisition. **Comondore Ravindran:** Methodology, Writing-Review & Editing, Project Administration.

References:

[1] Beeley, P.R. and Smart, R.F. eds., 1995. *Investment casting*. London: Institute of Materials.
[2] Kumar, P., Ahuja, I.S. and Singh, R., 2016. Effect of process parameters on surface roughness of hybrid investment casting. *Progress in Additive Manufacturing*, *1*(1), pp.45-53.
[3] Singh, S. and Singh, R., 2017. Some investigations on surface roughness of aluminium metal composite primed by fused deposition modeling-assisted investment casting using reinforced filament. *Journal of the Brazilian Society of Mechanical Sciences and Engineering*, *39*(2), pp.471-479.
[4] Brisotti, M.B., Garcia, L.D.F.R., Consani, S. and Pires-de-Souza, F.D.C.P., 2009. Influence of investment granulometry on the castability and surface roughness of castings obtained with Ni/Cr alloys. *Materials Research*, *12*, pp.169-172.
[5] Rath, S., Baumeister, G. and Hausselt, J., 2006. Investments for casting micro parts with base alloys. *Microsystem technologies*, *12*(3), pp.258-266.
[6] Jiang, J. and Liu, X.Y., 2007. Dimensional variations of castings and moulds in the ceramic mould casting process. *Journal of materials processing technology*, *189*(1-3), pp.247-255.
[7] Singh, S. and Singh, R., 2016. Fused deposition modelling based rapid patterns for investment casting applications: a review. *Rapid Prototyping Journal*.
[8] Kang, J.W. and Ma, Q.X., 2017. The role and impact of 3D printing technologies in casting. *China Foundry*, *14*(3), pp.157-168.
[9] Chhabra, M. and Singh, R., 2011. Rapid casting solutions: a review. *Rapid Prototyping Journal*.
[10] Reeves, P.E. and Cobb, R.C., 1997. Reducing the surface deviation of stereolithography using in-process techniques. *Rapid prototyping journal*.
[11] Di Angelo, L., Di Stefano, P. and Marzola, A., 2017. Surface quality prediction in FDM additive manufacturing. *The International Journal of Advanced Manufacturing Technology*, *93*(9), pp.3655-3662.
[12] Ahn, D., Kim, H. and Lee, S., 2009. Surface roughness prediction using measured data and interpolation in layered manufacturing. *Journal of materials processing technology*, *209*(2), pp.664-671.
[13] Mueller T., Tanner C., Improvements in the Burnout Process for Printed Patterns. *Investment Casting Institute.*
[14] Ahn, D., Kweon, J.H., Kwon, S., Song, J. and Lee, S., 2009. Representation of surface roughness in fused deposition modeling. *Journal of Materials Processing Technology*, *209*(15-16), pp.5593-5600.

[15] Tiwary, V.K., Arunkumar, P., Deshpande, A.S. and Rangaswamy, N., 2019. Surface enhancement of FDM patterns to be used in rapid investment casting for making medical implants. *Rapid Prototyping Journal*.
[16] Cheah, C.M., Chua, C.K., Lee, C.W., Feng, C. and Totong, K., 2005. Rapid prototyping and tooling techniques: a review of applications for rapid investment casting. *The International Journal of Advanced Manufacturing Technology*, *25*(3), pp.308-320.
[17] Singh, J., Singh, R. and Singh, H., 2018. Surface roughness prediction using Buckingham's Pi-theorem for SS-316L hip implant prepared as rapid investment casting. *Materials Today: Proceedings*, *5*(9), pp.18080-18088.
[18] Singh, R. and Singh, G., 2014. Investigations for statistically controlled investment casting solution of FDM-based ABS replicas. *Rapid Prototyping Journal*.
[19] Singh, R., Singh, S., Singh, I.P., Fabbrocino, F. and Fraternali, F., 2017. Investigation for surface finish improvement of FDM parts by vapor smoothing process. *Composites Part B: Engineering*, *111*, pp.228-234.
[20] Mueller T., Evaluation of a Low-Cost Material Extrusion Printer for Investment Casting Applications. *Investment Casting Institute*.
[21] Mueller T., Meyer A., Evaluation of a Low-Cost 3D Printer for Investment Casting Applications. *Investment Casting Institute.* Annual Technical Exposition St. Louis, 66th Conference& Exposition St. Louis, Missouri
[22] Investment casting made easy with desktop 3D printing. (2019, Feb 28). *PR Newswire*
[23] Investment Casting with PolyCast™. *Polymaker Application Note*.
[24] Jesiotr, M. and Myszka, D., 2013. Thermal Analysis of Selected Polymer Materials for Precision Casting Models. *Archives of Foundry Engineering*, *13*(2 spec.), pp.61-64.
[25] Hafsa, M.N., Ibrahim, M., Wahab, M. and Zahid, M.S., 2014. Evaluation of FDM pattern with ABS and PLA material. In *Applied Mechanics and Materials* (Vol. 465, pp. 55-59). Trans Tech Publications Ltd.
[26] Yao, W.L. and Leu, M.C., 2000. Analysis and design of internal web structure of laser stereolithography patterns for investment casting. *Materials & Design*, *21*(2), pp.101-109.
[27] Yao, W.L. and Leu, M.C., 1999. Analysis of shell cracking in investment casting with laser stereolithography patterns. *Rapid Prototyping Journal*.
[28] Alfred, T.S., 2000. Investment casters discuss RP, ceramic shell strength [J]. *Mod em Casting*, *1*, pp.38-40.
[29] ISO 4287: Geometrical Product Specifications (GPS) – Surface texture: Profile method – Terms, definitions and surface texture parameters (ISO 4287, 1997).
[30] Eustathopoulos, N., Nicholas, M.G. and Drevet, B. eds., 1999. Wettability at high temperatures. Elsevier.
[31] Marumo, C., 1975. Reactions and wetting behavior in the molten aluminum-fused silica system.
[32] Campbell, J., 1995. Review of fluidity concepts in casting. Cast Metals, 7(4), pp.227-237.
[33] Molina, J.M., Voytovych, R., Louis, E. and Eustathopoulos, N., 2007. The surface tension of liquid aluminium in high vacuum: the role of surface condition. International journal of adhesion and adhesives, 27(5), pp.394-401.
[34] Dezellus, O. and Eustathopoulos, N., 2010. Fundamental issues of reactive wetting by liquid metals. Journal of Materials Science, 45(16), pp.4256-4264.

[35] Unwin, J., Coldwell, M.R., Keen, C. and McAlinden, J.J., 2013. Airborne emissions of carcinogens and respiratory sensitizers during thermal processing of plastics. Annals of Occupational Hygiene, 57(3), pp.399-406.
[36] Turner, A., Arnold, R. and Williams, T., 2020. Weathering and persistence of plastic in the marine environment: Lessons from LEGO. Environmental Pollution, 262, p.114299.
[37] Morão, A. and De Bie, F., 2019. Life cycle impact assessment of polylactic acid (PLA) produced from sugarcane in Thailand. Journal of Polymers and the Environment, 27(11), pp.2523-2539.
[38] Brendgen, R., Graßmann, C., Grethe, T., Mahltig, B. and Schwarz-Pfeiffer, A., 2021. Coatings with recycled polyvinyl butyral on polyester and polyamide mono-and multifilament yarns. Journal of Coatings Technology and Research, 18(3), pp.819-829.
[39] Dhaliwal, A.K. and Hay, J.N., 2002. The characterization of polyvinyl butyral by thermal analysis. Thermochimica Acta, 391(1-2), pp.245-255.